

# H I and star formation in the most metal-deficient galaxies

Ekta,<sup>1\*</sup> Jayaram N. Chengalur,<sup>1\*</sup> Simon A. Pustilnik<sup>2\*</sup>

<sup>1</sup> National Centre for Radio Astrophysics, Post Bag 3, Ganeshkhind, Pune 411 007, India

<sup>2</sup> Special Astrophysical Observatory of RAS, Nizhniy Arkhyz, Karachai-Circasia 369167, Russia

Accepted 2008 . Received 2007

## ABSTRACT

We present Giant Metrewave Radio Telescope (GMRT) observations for three (viz., DDO 68, SDSS J2104–0035 and UGC 772) of the six most metal-deficient actively star-forming galaxies known. Although there is a debate as to whether these galaxies are undergoing their first episode of star formation or not, they are ‘young’ in the sense that their ISM is chemically unevolved. In this regard, they are the nearest equivalents of young galaxies in the early Universe.

All three galaxies, that we have observed, have irregular H I morphologies and kinematics, which we interpret as either due to tidal interaction with neighbouring galaxies, or the consequences of a recent merger. The remaining three of the six most metal-deficient galaxies are also known to have highly disturbed H I distributions and are interacting. It is interesting because these galaxies were chosen solely on the basis of their metallicity and not for any particular signs of interaction. In this sense (i.e., their gas has not yet had time to settle into a regular disc), one could regard these extremely metal deficient (XMD) galaxies as ‘young’. The current star formation episode is likely to have been triggered by interaction/merger. It is also possible that the tidal interaction has lead to enhanced mixing with metal-poor gas in outer disc, and hence to a low gas-phase metallicity in the central star-forming regions.

We also try to determine the threshold gas-density for star-formation in our sample of galaxies, and find that in general these galaxies do not show a one-to-one correspondence between regions of high H I column density and regions with current star formation. However, to the extent that one can define a threshold density, its value ( $\sim 10^{21}$  atoms  $\text{cm}^{-2}$ ) is similar to that in galaxies with much higher metallicity. The highest column densities that we detect in regions far outside star-forming regions (i.e., a lower limit to the star-formation threshold) are  $\sim 2 \times 10^{21}$  atoms  $\text{cm}^{-2}$ .

**Key words:** galaxies: dwarf – galaxies: individual: DDO 68 (UGC 5340) – galaxies: individual: SDSS J2104–0035 – galaxies: individual: UGC 772 – galaxies: kinematics and dynamics – radio lines: galaxies

## 1 INTRODUCTION

Blue Compact Galaxies (BCGs) were first identified by Zwicky (1965) as unusual members of the extragalactic zoo. A subset of them were later recognized to be nearby low-mass galaxies. Sargent & Searle (1970) found that the giant H II regions in BCGs have low metal-content and blue colours, typical of young (<10 Myr) stellar populations. As luck would have it, the first well studied BCGs, viz., I Zw 18 and II Zw 40 turned out to be fairly unrepresentative of the BCG class. Even after 30 years of study of BCGs, I Zw 18 continued to hold the record for the lowest metallicity, while II Zw 40 is a galaxy pair in an advanced state of merger,

which in general is not characteristic of BCGs. Partly because of the extreme properties of these two BCGs, and also because of the other unusual properties of the BCG class as a whole, it was hypothesized that some BCGs, including I Zw 18, may be undergoing their first burst of star formation. However, this was quickly recognized as being unlikely, since it was found that the outer parts of many BCGs have red colours, typical of a normal old stellar population.

None the less the idea that a small fraction of BCGs, particularly those with very low metallicity (i.e., the extremely Metal-Deficient (XMD) galaxies, with  $12 + \log(\text{O}/\text{H}) < 7.65$ , or  $Z < Z_{\odot}/10$ ; see Kunth & Östlin (2000) for a review), could be undergoing their first burst of star formation remained popular. In particular, deep photometry of the unresolved stellar population in outer parts

\* ekta@ncra.tifr.res.in,chengalu@ncra.tifr.res.in,sap@sao.ru

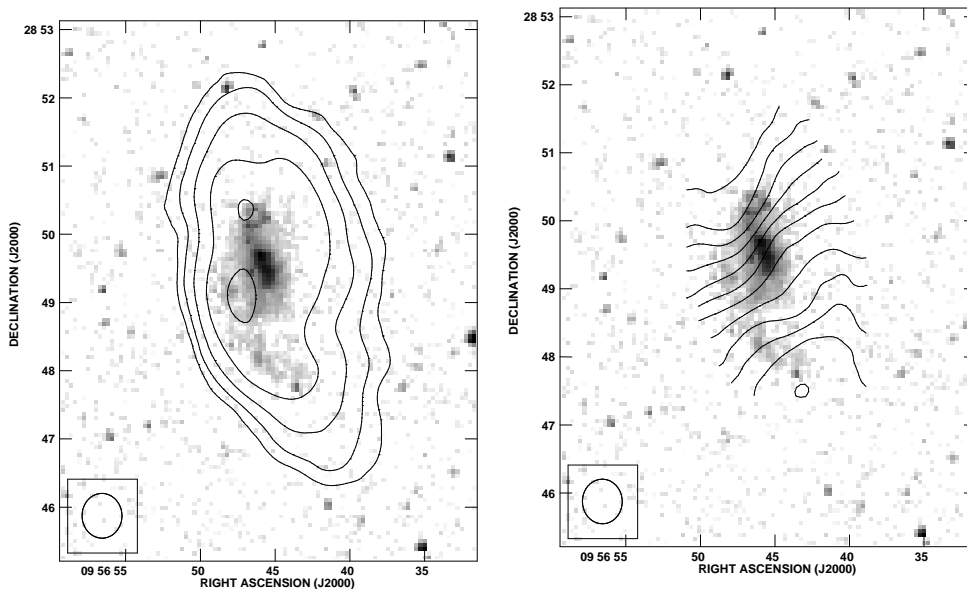


**Figure 1.** (a.) The integrated H I emission map of DDO 68 (in contours), at an angular resolution of  $\sim 39 \times 35$  arcsec<sup>2</sup>, is overlaid on *B*-band *DSS-II* optical image (grey-scale). The contours are at H I column densities of 7.8, 18.3, 42.8, 99.0 and  $233.9 \times 10^{19}$  atoms cm<sup>-2</sup>. The grey-scale is in arbitrary units. (b.) The H I velocity field at same resolution (contours) overlaid on same grey-scale image as in (a). The contours are from 462 to 541 km s<sup>-1</sup>, (from south to north) placed at regular intervals of 6.6 km s<sup>-1</sup>.

of several XMD BCGs shows no evidence for an old stellar population, e.g., I Zw 18 (Papaderos et al. 2002), SBS 0335-052 E, W (Papaderos et al. 1998; Pustilnik, Kniazev & Pramskij 2004, but see also Östlin & Kunth 2001), Tol 65 (Papaderos et al. 1999) and DDO 68 (Pustilnik, Kniazev & Pramskij 2005; Pustilnik, Tepliakova & Kniazev 2007). However, resolved CMD are essential to convincingly establish that the current episode of star formation is the first one. The case of I Zw 18 has been particularly tortuous. From *HST* WFPC2 (Aloisi, Tosi & Greggio 1999) and NICMOS (Östlin 2000) observations of this galaxy, it was argued that I Zw 18 contains AGB stars older than 1 Gyr and is hence not undergoing its first episode of star formation. However using deeper *HST* ACS observations, Izotov & Thuan (2004) concluded that I Zw 18 lacked RGB stars and was a bona fide young galaxy. Reanalysis of the same data by other groups indicated that RGB stars were, in fact, present (Momany et al. 2005; Tosi et al. 2006). More recently, Aloisi et al. (2007) analysed deeper *HST* images of I Zw 18 and convincingly established the presence of an RGB population, and hence that I Zw 18 has been forming stars for  $\gtrsim 2$  Gyr. One more XMD BCG, SBS 1415+437, which was initially claimed to be a candidate young galaxy (Thuan, Izotov & Foltz (1999); but see also Guseva et al. (2003), who reached a significantly more limited conclusion: viz., its low surface brightness (LSB) component luminosity-weighted age is probably not greater than 1-2 Gyr), was also found on the basis of *HST* based colour-magnitude diagram (CMD) analysis, to have an RGB population with age  $\gtrsim 1.3$  Gyr (Aloisi et al. 2005). Similar deep CMD data on the above-mentioned candidate young galaxies are

needed to rigorously test for the presence of an older stellar population.

However, regardless of whether XMD galaxies are undergoing their first episode of star formation, or not, the fact remains that they represent the most metal-poor sites of on-going star formation. In this sense, they can still be expected to provide useful insight into the processes that are relevant in galaxies at high redshift. For example, a comparison of the relation between the gas distribution and star formation in these galaxies with the observed relation in high-metallicity galaxies could help determine what, if any, systematic differences there are between star formation in high- and low-metallicity gas. In our continuing series of studies of H I in XMD galaxies (Chengalur et al. 2006; Ekta, Chengalur & Pustilnik 2006; Pustilnik & Martin 2007), we present Giant Metrewave Radio Telescope (GMRT) H I 21 cm observations of three of the six most metal-poor BCGs known. Global properties of the sample galaxies are briefly discussed in Section 2, and the observations are described in Section 3. The morphology and kinematics of gas in these galaxies is in itself interesting, and is discussed in Section 4. In Section 5, we use optical broad-band and/or H $\alpha$  images (taken from the published literature) as tracers of star formation (SF), to try to determine the relation between SF and the gas surface-density. In Section 6, we combine our results with those already obtained for other XMD galaxies, and compare them with those obtained from similar studies of more metal-rich galaxies. Finally, in Section 7, we summarise our results.

**Table 1.** Parameters of the GMRT observations

	DDO 68	J 2104-0035	UGC 772
Date of observations	2005 November 19, 20	2006 June 07	2006 November 25
Field center R.A.(2000)	09 <sup>h</sup> 56 <sup>m</sup> 45.7 <sup>s</sup>	21 <sup>h</sup> 04 <sup>m</sup> 55.3 <sup>s</sup>	01 <sup>h</sup> 13 <sup>m</sup> 40.4 <sup>s</sup>
Field center Dec.(2000)	28°49′35.0″	-00°35′21″	00°52′39.0″
Central Velocity (km s <sup>-1</sup> )	503	1401	1157
Time on-source (h)	~10	~6	~7.5
Number of channels	128	128	128
Channel separation (km s <sup>-1</sup> )	~3.3	~3.3	~3.3
Flux Calibrators	3C48, 3C286	3C286	3C48
Phase Calibrators	0824+185, 1111+119	2130+050	0519+001, 0204-170
Resolution (arcsec <sup>2</sup> ) (rms (mJy Bm <sup>-1</sup> ))	39 × 35 (1.6)	29 × 25 (1.7)	29 × 25 (1.7)
	27 × 22 (1.1)	17 × 11 (1.4)	34 × 26 (1.8)
	12 × 10 (1.0)	10 × 7 (1.2)	15 × 10 (1.2)
	8 × 7 (0.9)	7 × 5 (1.0)	8 × 7 (1.1)

## 2 THE SAMPLE

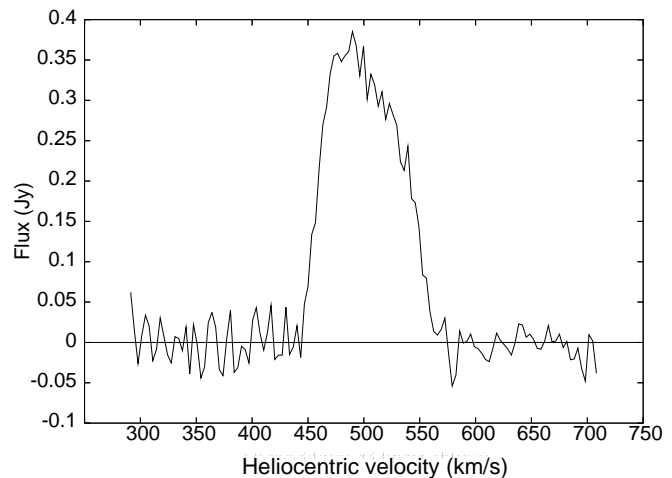
Fresh GMRT observations were obtained for three of the six most metal-deficient actively star-forming galaxies known, viz., DDO 68, UGC 772 and SDSS J2104-0035. Their optical appearance is dominated by the current starburst which is responsible for their blue colours. DDO 68 (UGC 5340,  $M_B \sim -14.54$ , discussed below) was identified as an XMD galaxy as part of a survey for dwarfs in the region of a nearby Lynx-Cancer minivoid (Pustilnik et al. 2005), while the remaining two galaxies were identified as XMD objects from a search through the SDSS DR4 data for metal-poor emission-line galaxies (Izotov et al. 2006a).

Pustilnik et al. (2005) found that the oxygen abundance of DDO 68 is  $12 + \log(\text{O}/\text{H}) \sim 7.21 \pm 0.03$ , which is in reasonable agreement with (albeit slightly higher than) that measured by Izotov & Thuan (2007) (weighted-average  $\sim 7.14 \pm 0.03$ ). It is the nearest of the 6 lowest metallicity XMD galaxies, with an estimated distance of 6.5 Mpc (Pustilnik et al. 2005).<sup>1</sup> The same authors present  $V$ ,  $R$  and  $H\alpha$  images for DDO 68, and draw attention to its peculiar optical morphology, which consists of central elongated region with a long curved tail extending to the south. The  $B$  magnitude given in Pustilnik et al. (2005) is  $m_B = 14.60$ , which corresponds to  $M_B = -14.54$ , at distance of 6.5 Mpc.

Izotov et al. (2006) measured oxygen abundances of  $12 + \log(\text{O}/\text{H}) = 7.17 \pm 0.09$  (updated to  $7.24 \pm 0.05$  by Izotov & Thuan (2007)) and  $7.26 \pm 0.03$  for UGC 772 and SDSS J2104-0035 (J2104-0035 in the rest of paper, for brevity), respectively. It should be noted that for UGC 772 oxygen abundance of only one of its several H II regions has been determined using the direct method.

UGC 772 is part of a loose group of galaxies, dominated by a SAB(s)m galaxy, NGC 428. It has a radial velocity of  $1157 \text{ km s}^{-1}$  (Smoker, Davies & Axon 1996), which corresponds to a Hubble-flow distance of  $\sim 16$  Mpc. At this distance, an apparent blue magnitude of 16.28 (Smoker et al. 1996) corresponds to  $M_B \sim -14.8$ .

J2104-0035 has a radial velocity of  $1401 \text{ km s}^{-1}$ , which for Hubble constant of  $70 \text{ km s}^{-1} \text{ Mpc}^{-1}$  corresponds to a


**Figure 2.** The integrated H I spectrum of DDO 68 made from spectral cube at angular resolution of  $\sim 39 \times 35 \text{ arcsec}^2$ .

distance of 20 Mpc. In section 4.2 below, we estimate its absolute blue magnitude to be  $M_B \sim -13.7$ .

## 3 OBSERVATIONS AND DATA REDUCTION

The details of the GMRT observations are given in Table 1. All the data were analysed using the AIPS software package. The major steps in the data analysis were (1) flagging of bad data points, (2) flux and phase calibrations, (3) bandpass calibration, (4) subtraction of continuum emission using UVSUB, (5) combining visibility files (in the case of multiple observing runs) using DBCON, (6) imaging and cleaning using the task IMAGR, (7) subtraction of any residual continuum using IMLIN. The imaging and cleaning process was done at a variety of resolutions, see Table 1 for details. Note, that since the GMRT has a hybrid configuration (Swarup et al. 1991), images at resolutions ranging from  $\sim 40$  to 4 arcsec can be made from data from a single observing run. Integrated H I 21 cm emission and velocity fields were generated from the data cubes using the task MOMNT. J2104-0035 was also observed using the Multibeam receiver of the Parkes radio telescope.

<sup>1</sup> The peculiar velocity flow in the vicinity of the Lynx-Cancer void makes distance to DDO 68 uncertain (Tully et al. 2008).

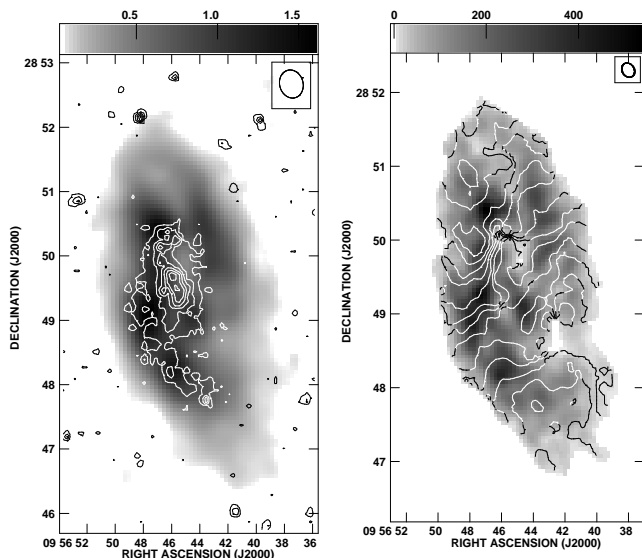


**Figure 3.** (Left) The integrated H I emission map of DDO 68, at an angular resolution of  $\sim 27 \times 22$  arcsec<sup>2</sup>, in grey-scale, over a range of  $1.0 - 33 \times 10^{20}$  atoms cm<sup>-2</sup>. A *B*-band *DSS-II* optical image is overlaid, in contours, in arbitrary units. (Right) The H I velocity contours of DDO 68 at an angular resolution of  $\sim 12'' \times 10''$  overlaid on integrated H I emission map (grey-scale) at same resolution. The contour levels are from 458 to 543.8 km s<sup>-1</sup> and are regularly spaced at 6.6 km s<sup>-1</sup>. The grey-scale is over the range of 0 to 534 Jy Beam<sup>-1</sup> ms<sup>-1</sup> ( $N_{HI} \sim 5.4 \times 10^{21}$  atoms cm<sup>-2</sup>).

## 4 H I MORPHOLOGY AND KINEMATICS

### 4.1 DDO 68

DDO 68 has been previously observed at the Westerbork Synthesis Radio Telescope (WSRT) by Stil & Israel (2002). Their maps (which have a relatively high resolution of  $\sim 13.5$  arcsec), by and large, trace only the peaks in the H I column density distribution and resolve out emission from the more extended, low-column-density gas seen in the low-resolution GMRT images (e.g., Fig. 1). As can be seen in the figure, the H I emission is significantly more extended than the optical emission. H I emission corresponding to the optical tail to the south can also be clearly seen. Finally, the H I distribution cuts off quite sharply on the eastern side, while it falls off much more gradually to the west. At the same resolution, the velocity field (Fig. 1) is, to zeroth order, consistent with that expected from a rotating gas-disc, however, deviations from axi-symmetry can also be seen. For example, the contours in the northern half of the galaxy are more open than those in the southern half. The H I spectrum of DDO 68 (obtained from the spectral cube at this same angular resolution) is shown in Fig. 2. The total H I flux that we measure from this spectrum is  $28.9 \pm 3$  Jy km s<sup>-1</sup>, which matches, within the error bars, with the value of 26.1 Jy km s<sup>-1</sup> measured by Stil & Israel (2002). For our assumed distance of 6.5 Mpc, the H I mass is  $2.9 \times 10^8 M_{\odot}$ . Like most other XMDs, DDO 68 is gas-rich –  $M_{HI}/L_B \sim 2.9$ .

In Fig. 3 we show a higher-resolution ( $\sim 27 \times 22$  arcsec<sup>2</sup>)

**Table 2.** Velocity widths in DDO 68

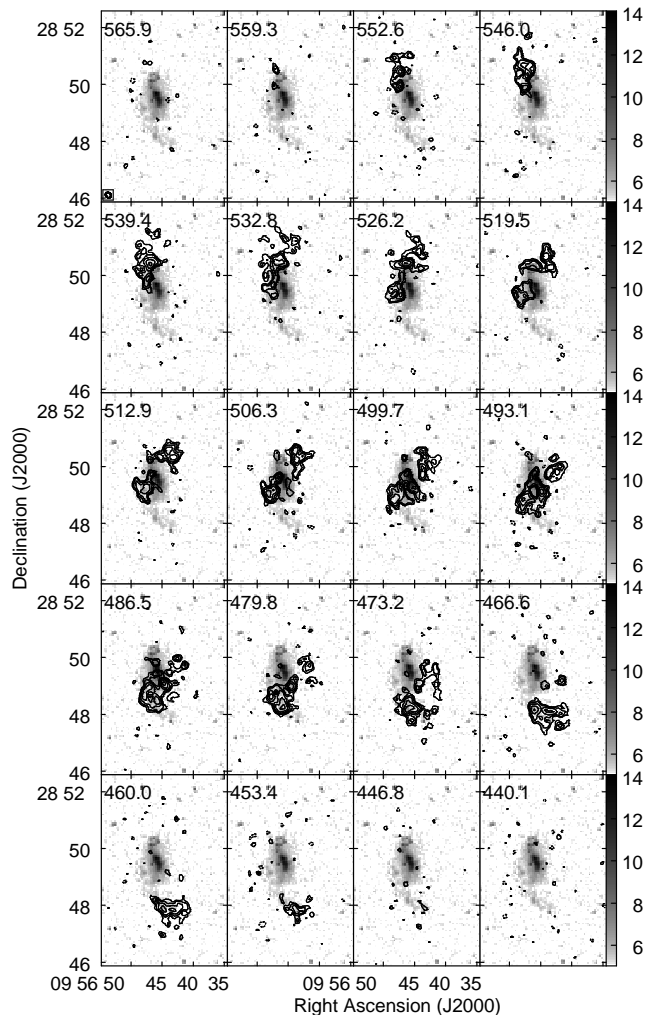
Region	Stil (1999) (km s <sup>-1</sup> )	GMRT (22 arcsec) (km s <sup>-1</sup> )	GMRT (12 arcsec) (km s <sup>-1</sup> )
1	16.7	12.7	10.5
2	18.3	17.0	14.4
3	14.4	10.4	9.6

image of the integrated H I emission (grey-scale) with the *B*-band *DSS-II* optical image overlaid as contours. At this resolution one can see that the galaxy has two massive H I arms, North-East-South (NES) and South-West-North (SWN), which wind around the main stellar body. The southern part of NES arm is coincident with the optical tail, while SWN arm has no obvious optical counterpart. Since it is highly unusual for a dwarf galaxy to have spiral arms, we interpret these structures (see below) to be tidal tails in a putative merger remnant. In addition to these arms/tails, there is H I emission that roughly coincides with the central stellar body, but its western part corresponds to regions with very low H I column density.

To better understand the connections between the optical and H I structures, it is instructive to look at the H I channel-maps. Fig. 4 shows channel maps, at resolution of  $\sim 12 \times 10$  arcsec<sup>2</sup>, overlaid on a grey-scale representation of the *B*-band *DSS-II* optical image. One can see that the H I emission that is coincident with the 'southern' optical tail actually starts at the northern end of the galaxy, at velocities around 553 km s<sup>-1</sup>. As the velocity decreases, the emission from this NES arm moves southward along the eastern side of the main body of optical emission, and then finally forms the long arcing tail to the south. In the lowest velocity channel maps, one can see that the H I emission extends to much larger galacto-centric distances than the corresponding stellar emission. In the channel maps one can also discern the two other H I features seen in Fig. 3, viz., the H I associated with the central body of the galaxy and the SWN H I arm. Note, however, the overlap of H I is largely on the eastern side of optical galaxy – the western part of the central stellar emission has very little gas associated with it. The SWN arm starts at the southern end of the galaxy (466 km s<sup>-1</sup>), and moves northwards as the velocity increases. From the high-resolution velocity field (Fig. 3), one can see that there is reasonable continuity in the velocity field as one goes along the arms, but that there are velocity discontinuities between the arms and the central body.

We obtained maximum rotational velocities of 55 and 48 km s<sup>-1</sup> at 144 and 168 arcsecs, respectively, while trying to derive rotation curves for approaching and receding sides (not shown). Given the disturbed, asymmetric nature of the velocity field these can only be regarded as indicative rotation curves. The implied dynamical mass (average of the results for the receding and approaching sides) is  $\sim 3.2 \times 10^9 M_{\odot}$ .

The velocity dispersion is an important parameter for systems like DDO 68, since in the process of merging the gas is expected to be agitated (Elmegreen, Kaufman & Thomasson 1993). Stil (1999) found an enhanced velocity dispersion in some regions of DDO 68. We estimated this parameter from our GMRT



**Figure 4.** The HI channel maps of DDO 68, at an angular resolution of  $\sim 12 \times 10$  arcsec<sup>2</sup>, overlaid on a *B*-band *DSS*-II optical image, in grey-scale. The contour levels are at -3, 3, 4.2, 6.0, 8.5 and 12.0 times the rms noise in single channel, which is 1.1 mJy beam<sup>-1</sup>. Every alternate channel is shown and corresponding velocity, in units of km s<sup>-1</sup>, is labelled.

data via Gaussian fitting in three of four regions shown by Stil (1999), which we could identify. Our data for two beamsizes are shown in Table 2 along with those of Stil (1999). As seen from this table, GMRT data give significantly smaller widths, which in turn decrease with decrease of beamsize. The largest width (Region 2) corresponds to the place of overlap between the ‘tidal’ arm and the main body. The velocity width in these regions is hence likely to be enhanced because of bulk motions. Thus our data do not support the proposition that there is a significant enhancement of velocity dispersion in this galaxy. Our upper limits imply that they, at most, can be enhanced by 30–40 per cent relative to the standard value of 7–8 km s<sup>-1</sup>.

This could have important implications for modelling of gas agitation in the process of strong interactions/mergers. DDO 68 would be an excellent candidate for comparing numerical models of gas-rich, low-mass mergers with observations.

## 4.2 SDSS J2104–0035

The *g*-band SDSS image of J2104–0035 is shown in Fig. 5. The optical emission is dominated by two bright star-forming knots, one at the northern edge of the galaxy and the other near the centre. Izotov et al. (2006) note that its appearance is similar to that of ‘cometary’ blue compact dwarf galaxies (e.g., Mkn 59, Mkn 71 (Noeske et al. 2000)), which have a bright star-forming region at one end of an elongated stellar body. This unusual morphology has been suggested to be a consequence of propagating star formation (Noeske et al. 2000). The cometary morphology, combined with the fact that there is a bright star superposed on the north-western edge of J2104–0035, makes it difficult to determine the galaxy’s surface brightness profile. The total magnitude  $B_{\text{tot}}$  calculated from the total SDSS *u, g, r* magnitudes is 18.07, which corresponds to  $M_B \sim -13.7$ , at our adopted distance of 20 Mpc. Fitting (adopting an inclination of 70 degrees, as measured from the axial ratio of the *g*-band image) only to the southern LSB half of the galaxy, (i.e., excluding the star-forming regions) one gets a *B*-band scale-length of 2.3 arcsec, and an (extrapolated) Holmberg radius of 9.8 arcsec ( $\sim 0.95$  kpc).

The low ( $29 \times 25$  arcsec<sup>2</sup>) resolution HI emission map (Fig. 5) shows that the HI in J2104–0035 is very extended compared to the optical emission. At a column density of  $2 \times 10^{19}$  atoms cm<sup>-2</sup>, the HI extends to  $\sim 5.3$  times the Holmberg radius (i.e., an extent comparable to that of DDO 154 (Carignan & Purton 1998), though somewhat smaller than that of NGC 3741, the current record holder for the most extended HI envelope (Begum, Chengalur & Karachentsev 2005)). The comparison may not be apt, since unlike the case for the latter two galaxies, the HI in J2104–0035 is not in a regular disc. The HI distribution instead looks disturbed with extensions to the south and east. From the synthetic HI spectrum (Fig. 6), we measure an HI flux of  $\sim 1.5 \pm 0.15$  Jy km s<sup>-1</sup>. Overlaid on this spectrum is the spectrum obtained at Parkes, for which the integrated flux is  $2.0 \pm 0.2$  Jy km s<sup>-1</sup>. The two measurements do not overlap within the error bars, suggesting that the galaxy has a diffuse HI component that has been resolved out at the GMRT. At a distance of  $\sim 20.0$  Mpc, the Parkes flux corresponds to a total HI mass of  $\sim 1.9 \pm 0.2 \times 10^8 M_{\odot}$ , and a very large  $M_{\text{HI}}$  to  $L_B$  ratio of  $\sim 4.1 \pm 0.4$ . A Gaussian fit to the Parkes spectrum gives a central velocity of 1401 km s<sup>-1</sup> and a velocity width of 64 km s<sup>-1</sup>.

At higher resolutions (e.g., Fig. 7) the HI emission is a closer match to the optical morphology. The HI emission, however, remains disturbed-looking with extensions to the south and east.

The intensity-weighted velocity field of J2104–0035, at angular resolution of  $\sim 29 \times 25$  arcsec<sup>2</sup>, is shown in Fig. 5. Although there is an overall velocity gradient from north to south, there is substantial asymmetry between the northern and southern halves of the galaxy. At the northern tip of the

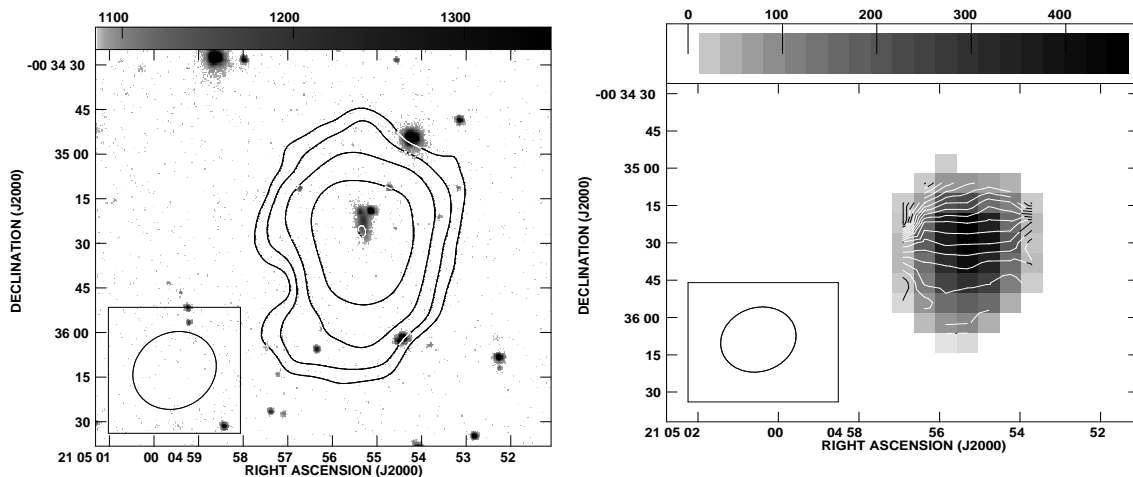


**Figure 5.** (Left.) The integrated H I map of J2104-0035, in contours, at an angular resolution of  $\sim 29 \times 25$  arcsec<sup>2</sup>, overlaid on a *g*-band SDSS image (grey-scale in arbitrary units). The contour levels are at H I column densities of 5.1, 10.6, 22.3, 46.5,  $97.3 \times 10^{19}$  atoms cm<sup>-2</sup>. (Right.) The intensity-weighted H I velocity field of J2104-0035, in contours, overlaid on integrated H I map, in grey-scale, at same angular resolution. The contour levels are from 1365 (northern-most) to 1418 km s<sup>-1</sup> (southern-most). Grey-scale is at H I column densities from 0 to 455.0 Jy Beam<sup>-1</sup> ms<sup>-1</sup> (i.e.,  $N_{HI} \sim 7.7 \times 10^{20}$  atoms cm<sup>-2</sup>.)

galaxy the velocity gradient is particularly sharp. Given the large deviations of the velocity field from that expected from a rotating disc, we do not attempt to fit a rotation curve to it. Instead we compute an indicative dynamical mass using,

$$M_{ind} = 2.3 \times 10^5 \times R_{kpc} \times V_{kms}^2 M_{\odot}. \quad (1)$$

Assuming an inclination of 70 degrees, a velocity range of  $\sim 41$  km s<sup>-1</sup> and a radial extent of  $\sim 5.0$  kpc, gives an indicative dynamical mass  $M_{ind} \sim 2.4 \times 10^9 M_{\odot}$ .

### 4.3 UGC 772

The optical emission in UGC 772 (with  $M_B \sim 16.28$  (Smoker et al. 1996)) consists of two well-separated condensations; in the UGC catalog itself, the system is flagged as being ‘possibly two dwarfs in contact’. It is part of a small group of galaxies of which a SAB(s)m galaxy, NGC 428 is the dominant member (at heliocentric velocity of 1152 km s<sup>-1</sup> and with  $M_B \sim -19.2$ ). Smoker et al. (1996) present VLA H I observations of the NGC 428 field. Their maps have low signal-to-noise ratio at position of UGC 772 (which is at the edge of their imaged field), but they note that the galaxy may have an H I extension to south-east and that the system may represent the ongoing merger of two smaller dwarfs. They measure a heliocentric velocity of 1157 km s<sup>-1</sup> (which corresponds to a distance of  $\sim 15.1$  Mpc, after correcting for Virgo centric infall). At this distance the absolute magnitude is  $M_B \sim -14.74$ .

The synthetic H I spectrum of UGC 772 (produced from data at resolution of  $\sim 15 \times 10$  arcsec<sup>2</sup>) is shown in Fig. 8. From the spectrum we measure a heliocentric velocity of  $1157 \pm 1.7$  km s<sup>-1</sup> and a total integrated flux of  $5.3 \pm 0.4$  Jy km s<sup>-1</sup>, in good agreement with the single dish measurements of Smoker et al. (2000). From the GMRT ob-

**Table 3.** Main parameters of the observed galaxies.

Parameter	DDO 68	J2104-0035	UGC 772
$m_B$	14.6	18.07	16.28
$A_B^1$	0.08	0.28	0.122
$V_{hel}$ (km s <sup>-1</sup> )	502	1401	1157
D(Mpc)	6.5	20.0	15.1
$M_B$	-14.54	-13.7	-14.7
$12 + \log(O/H)$	$7.14 \pm 0.03$	$7.26 \pm 0.03$	$7.24 \pm 0.05$
H I flux (Jy km s <sup>-1</sup> )	28.9	2.0	5.3
$M_{HI}$ ( $10^8 M_{\odot}$ )	2.9	1.9	2.9
$M_{gas}$ ( $10^8 M_{\odot}$ )	3.8	2.5	3.8
$M_{HI}/L_B$	2.9	4.1	2.4

<sup>1</sup>  $A_B$  are the values of foreground Galactic extinction (Schlegel, Finkbeiner & Davis 1998) as given in NED.

servations, the H I mass is  $2.9 \pm 0.2 \times 10^8 M_{\odot}$ , and  $M_{HI}/L_B \sim 2.4$ .

Our low-resolution image (Fig. 9(Left.)) also shows the tentatively detected south-east H I extension in the VLA map of Smoker et al. (1996). In the channel maps (Fig. 10), these extensions can be seen only over relatively narrow velocity ranges (viz., 1186.9–1180.3 and 1147.0–1137.1 km s<sup>-1</sup>). At higher resolutions (e.g., at  $\sim 15 \times 10$  arcsec<sup>2</sup>, Fig. 9(Centre.)), the H I emission can be seen to have a central ‘hole’ surrounded by a broken high column density ‘ring’. The highest H I column density region of the ‘ring’ overlaps with the bright condensation to the south. Optical emission is present over the entire north western part of the ‘ring’; in contrast, eastern part of ‘ring’ does not appear to have any associated optical emission. However, on smoothing the optical emission to a resolution of  $\sim 7 \times 7$  arcsec<sup>2</sup>, one can see diffuse faint emission coincident with the eastern part of the ‘ring’.

The H I velocity map of UGC 772, at a resolution of

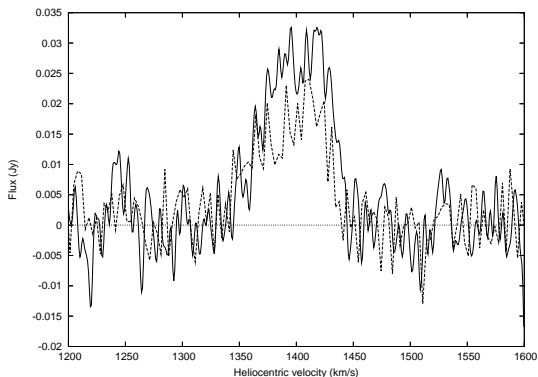


**Figure 6.** The H I spectrum of J2104-0035 obtained from the Parkes telescope (solid line) and the GMRT (dashed line).

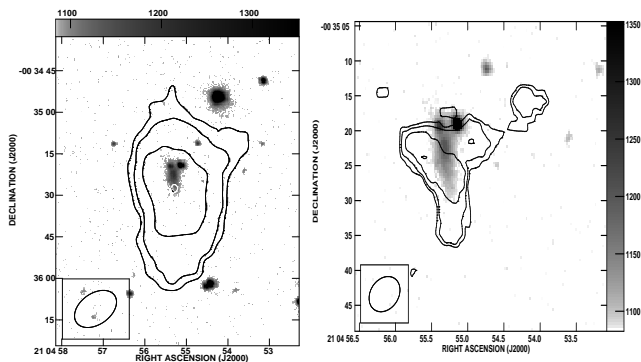


**Figure 7.** *Left.* The integrated H I map of J2104-0035, in contours, at an angular resolution of  $\sim 17 \times 11$  arcsec<sup>2</sup>, overlaid on a  $g$ -band SDSS image (grey-scale, in arbitrary units). The contour levels are at H I column densities of 1.0, 2.7, 7.1,  $19.2 \times 10^{20}$  atoms cm<sup>-2</sup>. *Right.* The integrated H I map of J2104-0035 at an angular resolution of  $\sim 7 \times 5$  arcsec<sup>2</sup>. The contour levels are at H I column densities of  $\sim 6.2$ , 11.0, 19.3 and  $33.8 \times 10^{20}$  atoms cm<sup>-2</sup>. The SDSS  $g$ -band image is shown in grey-scale, in arbitrary units.

$\sim 15 \times 10$  arcsec<sup>2</sup>, overlaid with H I integrated map at same resolution, is shown in Fig. 9(Right.). The velocity field is distorted and the outer parts are suggestive of a warp. We tried to derive rotation curve for approaching and receding sides (not shown). Leaving the inclination as a free parameter in the fit did not lead to meaningful results, hence the inclination was set to a value of 40 degrees, as obtained from the H I morphology and assuming an intrinsic axial ratio of 0.25. The maximum rotational velocities are 26 and 29 km s<sup>-1</sup>, at radial distances of 42 and 54 arcsecs, for approaching and receding sides, respectively. As for DDO 68, we caution that this rotation curve should only be treated as indicative. The derived (average of receding and approaching sides) dynamical mass is  $8.3 \times 10^8 M_{\odot}$ .

A larger-scale map of the field (Fig. 11) shows two more galaxies, viz., NGC 428 and MCG +00-04-049 (note that this image is not corrected for primary-beam attenuation). NGC 428 shows a tail to the south, which is better seen in the VLA data of Smoker et al. (1996), in which this galaxy is at the center of the field. This tail, the south-east exten-

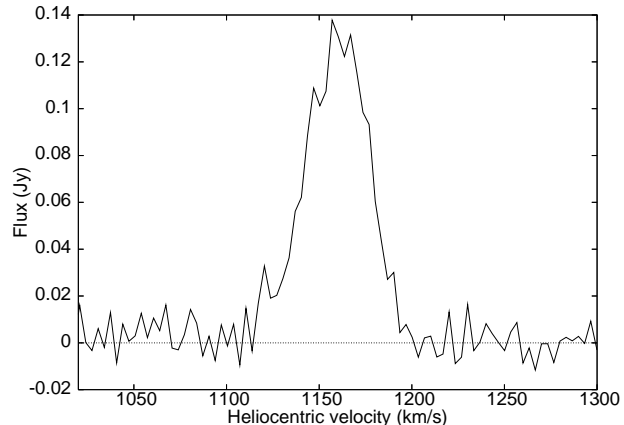


**Figure 8.** The integrated H I spectrum of UGC 772 obtained from data at a resolution of  $\sim 15 \times 10$  arcsec<sup>2</sup>.

sion in H I emission of UGC 772 (Figs. 9(Left.), 10) and the south-west tail-like extension in the outer H I contours of MCG +00-04-049 (Fig. 11(Left.)) strongly suggest that the galaxies in the group are tidally interacting.

## 5 STAR FORMATION

It has been suggested that star formation in dwarf galaxies occurs only when the gas column-density crosses a threshold value of  $\sim 10^{21}$  atoms cm<sup>-2</sup> (Skillman 1987; Taylor et al. 1994). If this is related to a threshold amount of dust shielding required for the production of molecular gas, one might expect that XMD galaxies would have a higher threshold column-density.

The H $\alpha$  image of DDO 68 (Pustilnik et al. (2005)), shows three separate regions of ongoing star formation, one in the central region, the second in the northern ring and the third in a ring-like H II region in the southern tail. On comparing the H $\alpha$  map with the H I column density at a resolution of  $\sim 8 \times 7$  arcsec<sup>2</sup> (linear resolution of  $\sim 250$  pc), we find that, in general (but not in all cases), the regions of ongoing star formation correspond to peaks in the H I column density. However, there are several H $\alpha$  emitting regions for which the gas surface-density (computed after multiplying the H I face-on column density by a factor of 1.3 to account for Helium) is lower (by a factor of  $\sim 2$ ) than the nominal threshold density of  $10^{21}$  atoms cm<sup>-2</sup>. Further, there are regions where the gas surface-density is substantially higher than that the threshold density (e.g., in the tail), but for which there is no corresponding H $\alpha$  emission.

In Fig. 7 we show a  $\sim 6.7 \times 4.7$  arcsec<sup>2</sup>-resolution ( $\sim 645 \times 459$  parsec<sup>2</sup>) map of the H I emission from the galaxy. Though both H II regions in J2104-0035 are close to high H I column density regions, Fig. 7 shows that they lie outside the region of highest H I column density. The gas surface-density at the northern H II region is only  $\sim 6.0 \times 10^{20}$  atoms cm<sup>-2</sup>. Further, there are H I peaks in western and southern H I extensions, at gas densities close to threshold, but with no corresponding optical emission.

For UGC 772, we calculated gas surface-densities at locations of the H II regions, from a map at an angular resolution of  $\sim 8 \times 7$  arcsec<sup>2</sup>, i.e.,  $\sim 600 \times 500$  pc<sup>2</sup>. The peak gas surface-density (computed assuming inclination

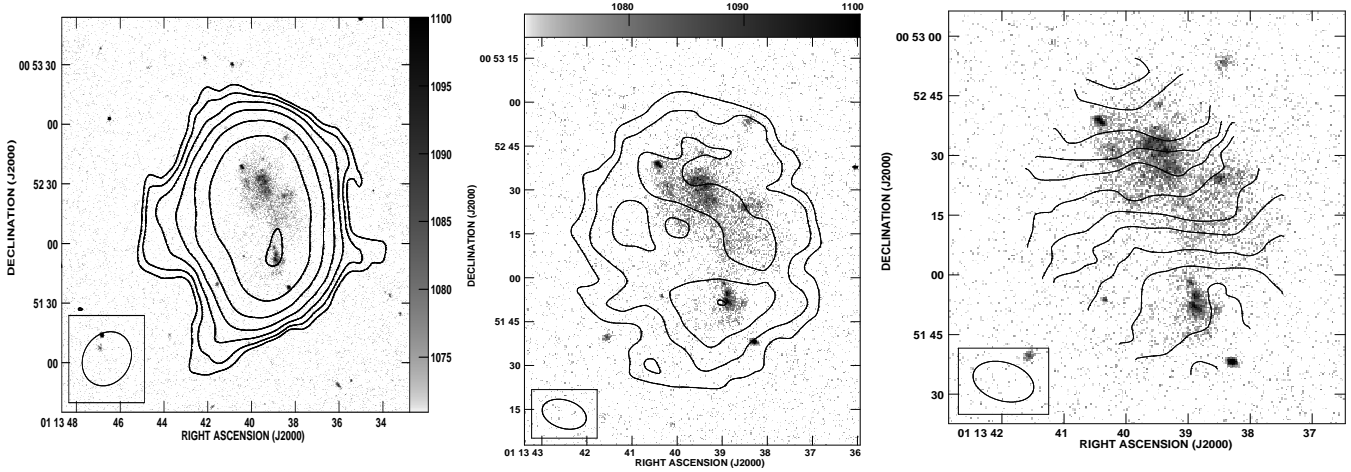


**Figure 9.** (Left.) The integrated H I emission map of UGC 772 (in contours), at an angular resolution of  $\sim 34 \times 26$  arcsec<sup>2</sup>. The contour levels are at H I column densities of 2.7, 5.2, 9.8, 18.4, 34.8, 65.8 and  $124.3 \times 10^{19}$  atoms cm<sup>-2</sup>. (Centre.) Integrated H I emission map of UGC 772, at a resolution of  $15 \times 10$  arcsec<sup>2</sup>. The contours are at 3.4, 6.6, 12.8,  $24.8 \times 10^{20}$  atoms cm<sup>-2</sup>. (Right.) Intensity weighted H I velocity field of UGC 772 field, in contours, at an resolution of  $\sim 15 \times 10$  arcsec<sup>2</sup>. The contours are equally spaced at velocity interval of 3.3 km s<sup>-1</sup>, in the range of 1140–1176 km s<sup>-1</sup>. All contours are overlaid upon SDSS *g*-band optical image in grey-scale (arbitrary units).

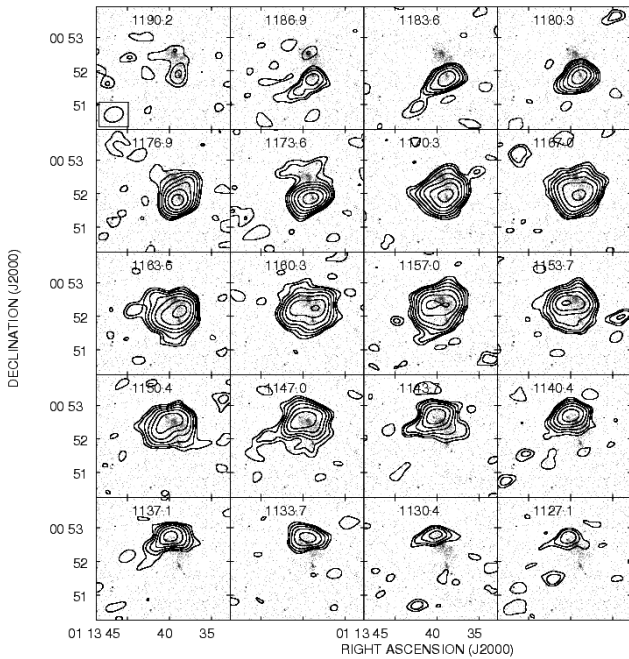


**Figure 10.** The channel maps of UGC 772, at an angular resolution of  $\sim 34 \times 26$  arcsec<sup>2</sup>, in contours. Velocity corresponding to each channel is labelled. Rms noise in single channel is 1.8 mJy beam<sup>-1</sup>. The contours are at -2, 2, 2.8, 4.0, 5.7, 8.0, 11.3 and 16.0 times rms. The SDSS *g*-band image is shown in grey-scale, in arbitrary units.

$\sim 42$  degrees)  $\sim 3.1 \times 10^{21}$  atoms cm<sup>-2</sup>), is associated with the southern optical condensation. H II regions, marked as 1 and 3 in Fig. 1 of Izotov & Thuan (2007), are associated with H I peaks at gas surface-densities  $\sim 1.9$  and  $1.2 \times 10^{21}$  atoms cm<sup>-2</sup>, respectively. On the other hand, the H II region 2 of Izotov & Thuan (2007) lies in the central H I ‘hole’, with a corresponding gas surface-density of  $\sim 5.6 \times 10^{20}$  atoms cm<sup>-2</sup>. Further, there are regions in the eastern part of the H I ‘ring’, which have gas surface-densities greater than  $2.0 \times 10^{21}$  atoms cm<sup>-2</sup>, but with no associated optical emission.

In summary for these three galaxies, a gas column density of  $\sim 10^{21}$  atoms cm<sup>-2</sup> does not appear to be either a necessary or sufficient condition for star formation. Note that in all cases, our spatial resolution is comparable or better than the  $\sim 500$  pc linear resolution used to determine the threshold density by Skillman (1987).

Schaye (2004) (see also Schaye (2007); Schaye & Dalla Vecchia (2008)) suggested that star formation is related to the formation of a cold phase of the interstellar medium, and gives fitting formulae for the threshold column density as a function of the gas fraction, pressure, metallicity, ionizing radiation flux, etc.. All other factors being equal, the threshold density increases with increasing gas fraction and decreasing metallicity. This would imply, on the face of it, that gas rich XMD galaxies should have a higher threshold for star formation than spirals. However as discussed in detail in Schaye (2004), for determining the star formation threshold in spirals, it is the conditions in the outer portions of the disc that are relevant. In these regions, the gas fraction and metallicity are not very different to that in XMD galaxies. If we assume that that in the outer parts of spiral discs, the gas fraction is 1.0, the thermal pressure accounts for half the total pressure, the metallicity is 0.1 times the solar metallicity



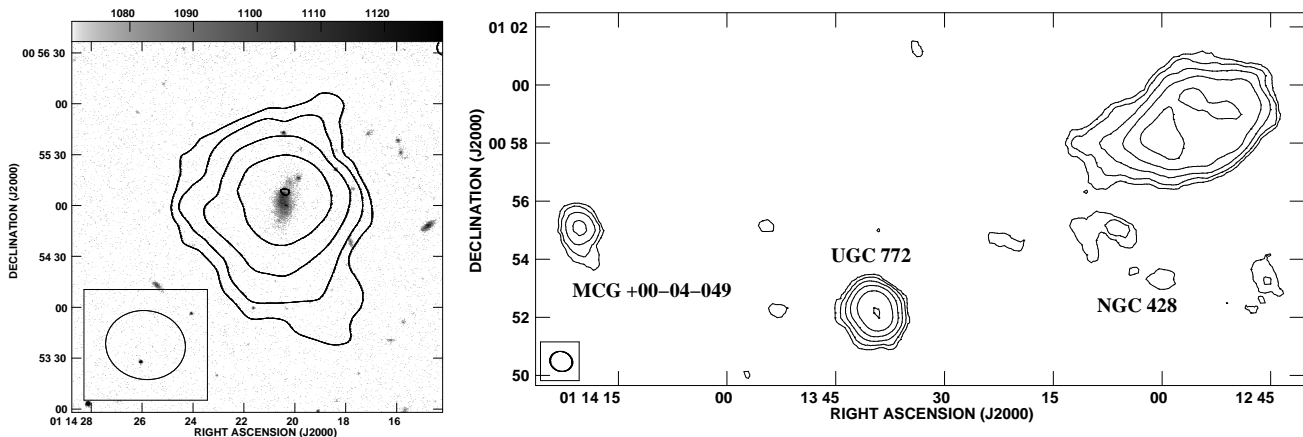


**Figure 11. (Left.)** Integrated HI emission map of MCG +00-04-049, in contours, at a resolution of  $\sim 46 \times 42$  arcsec<sup>2</sup> ( $\sim 3.2$  kpc<sup>2</sup>). The contour levels are at HI column densities of  $\sim 7.2, 12.3, 21.0, 35.9, 61.3$  atoms cm<sup>-2</sup>. The primary-beam gain-factor at position of MCG +00-04-049 is  $\sim 1.7$ . The *g*-band SDSS image is shown in grey-scale, in arbitrary units. **(Right.)** Integrated HI emission map of UGC 772 field at same resolution as in (left.). MCG +00-04-049 is seen in east, UGC 772 is central, while NGC 428 is the westernmost. The contour levels are at 65, 123, 234, 443, 843, 1600 Jy/B\*ms<sup>-1</sup>. 1 arcsec corresponds to a linear scale of  $\sim 73$  pc.

and the *UV* radiation intensity is  $10^6$  cm<sup>-2</sup>s<sup>-1</sup>, the expected threshold density from equation (23) of Schaye (2004) is  $\log(N_{HI}) \sim 20.84$ . On the other hand, for XMD galaxies, if we take that the gas fraction is  $\sim 1$ , the metallicity is  $\sim 0.03$  solar, but the ratio of thermal pressure to total pressure and the *UV* intensity are unchanged, the predicted threshold density is only a factor of  $\sim 1.4$  larger, i.e.,  $\log(N_{HI}) \sim 21$ . As such, it appears that a much larger sample will be required to test for the dependence of the threshold density on the gas-phase metallicity.

## 6 DISCUSSION

In Table 3, we summarise the main observed and derived parameters of the studied galaxies. Their *B*-band luminosities all fall within a factor of 2.5, with the average  $M_B \sim -14.3$ , while their  $M(HI)$  and  $M(HI)/L_B$  ratios differ by less a factor of 1.5 and 1.7, respectively. In this respect, they form a much more homogeneous sample than the sample of 22 XMD galaxies studied by Pustilnik & Martin (2007). Of course a sample of 3 is too small to draw any meaningful statistical conclusion, this homogeneity is suggestive of similar evolutionary path-ways for all three galaxies. All of the three galaxies that we have observed also have peculiar HI morphology and kinematics. UGC 772 is located in a loose group, and has easily identifiable neighbours which could be the cause of the observed disturbances. DDO 68, on the other hand, is located in a low-density region, in the periphery of the Lynx-Cancer void (Pustilnik et al. 2005). The Hubble flow around DDO 68 is very quiet. The radial velocities of all six dwarf galaxies within 500 kpc of it differ by less than 40 km s<sup>-1</sup>. The nearest neighbour of DDO 68, the dwarf galaxy UGC 5427, is located at a projected distance of  $\sim 200$  kpc and a radial velocity separation of 5 km s<sup>-1</sup>. UGC 5427 also has a somewhat disturbed appearance with a chain of bright knots in a spiral-arm like

feature, which makes it tempting to suggest that these two galaxies are tidally interacting. However, given its relatively large projected separation, it seems unlikely that tidal interaction with UGC 5427 is the cause of DDO 68's disturbed morphology. For example, if we assume that their true spatial separation and relative velocity are 200 kpc and  $\sim 50$  km s<sup>-1</sup>, respectively, then their close encounter could occur  $\sim 4$  Gyr ago. This is large compared to the ages ( $\sim 0.01$ –1 Gyr (Pustilnik et al. 2005; Pustilnik et al. 2007)) of the star-formation episodes in DDO 68.

If interaction with UGC 5427 is not the cause of DDO 68's disturbed morphology, then a remaining possibility is that DDO 68 represents the late-stage merger of two gas-rich progenitors, in which the gas is now settling down to form a disc. In this context, it is interesting to note that numerical simulations (e.g., Springel & Hernquist 2005) show that a disc galaxy can form in merger of extremely gas-rich progenitors. Mergers are not very rare among BCGs. E.g., Östlin et al. (2001) also interpret, from the disturbed optical morphology and H $\alpha$  kinematics of their sample of BCGs, that they are most likely the results of mergers. Similarly, Pustilnik et al. (2001b) assign  $\sim 15$  per cent of their sample BCGs as having a merger-like morphology.

We use a very approximate calculation below to show that the ages of the oldest stellar populations in DDO 68 ( $\sim 1$  Gyr), as derived by Pustilnik et al. (2007), match with the time of first encounter between its progenitors. Figure 11 of Springel, Di Matteo & Hernquist (2005) indicates that 'short' tails, like those of DDO68, are seen during later phases of merger (in comparison to the extended ones produced during the first encounter). Their ages are comparable to the rotation period of merging components and one-third of the time since the first encounter. Assuming that the velocity of tail relative to the systemic velocity of DDO 68 is  $\sim 50$  km s<sup>-1</sup> and its length is  $\sim 5$  kpc, age of tail is  $\sim 200$  Myr, which corresponds to a time since the first encounter of  $\sim 0.6$  Gyr.

We note, however, that although the morphology and large-scale kinematics of DDO 68 suggest that it could be an ongoing merger, its large gas-mass fraction, and the lack of evidence for an enhanced velocity dispersion are in conflict with the predictions of numerical models of mergers (Springel et al. (2005) and Elmegreen et al. (1993), respectively). In the Springel et al. (2005) models, the gas-fraction of the merger product is ( $f_{\text{gas}} \sim 0.2\text{--}0.3$ ), while DDO 68 is gas-rich ( $M_{\text{HI}}/L_B \sim 2.9$  (Table 3);  $f_{\text{gas}} \sim 0.95$  (Pustilnik et al. 2007)). These differences may be, in part, due to the fact that the masses of the putative progenitors of DDO 68 are roughly two orders of magnitude smaller than those of the model galaxies in the Elmegreen et al. (1993) and Springel et al. (2005) simulations, and in part, due to limitations in the star formation and feedback recipes used in the simulations. Given the importance of gas-rich low-mass mergers in the early universe, a detailed numerical model of DDO 68 would be particularly interesting.

J2104–0035 is also relatively isolated, and the only other galaxy within 500 kpc and  $500 \text{ km s}^{-1}$  from it is the compact dwarf emission-line galaxy SDSS J210347.23–004949.7 ( $M_B = -14.49$ ), which is at a projected distance of 22.3 arcmin ( $\sim 130$  kpc for our assumed distance of 20 Mpc) and has, within cited error bars of  $\sim 5 \text{ km s}^{-1}$ , the same redshift. This is the only likely candidate for having caused the observed disturbance in J2104–0035. Alternatively we conjecture that J2104–0035 may be a case of an advanced merger.

It is interesting to note that all three of our sample galaxies have disturbed morphology and kinematics. In this regard, they closely resemble the three lowest metallicity BCGs, viz., I Zw 18 and SBS 0035–052 E, W. Pustilnik et al. (2001a) show that SBS 0035–052 consists of an interacting pair of dwarf galaxies with a common H I envelope, while van Zee et al. (1998) show that I Zw 18 has a complex H I distribution, which they describe as a ‘fragmenting H I cloud in the early stages of galaxy formation’. Thus, although tidal interaction was not specifically selected for when searching for XMD BCGs, all six of the most metal-deficient galaxies have highly disturbed morphologies and kinematics. Indeed this seems to be a common feature for XMD BCGs (e.g., Chengalur, Giovanelli & Haynes 1995; Chengalur et al. 2006; Ekta et al. 2006).

Our, and past, results suggest that interactions/mergers could play an important role in triggering star formation in XMD galaxies. There are two factors that we can speculatively suggest as being responsible for this. The first is that intense SF episodes may occur only due to strong tidal disturbances (particularly, if the gas discs are less susceptible to internal instabilities, see the discussion below). The second is that tidal interaction could lead to a more efficient large-scale mixing of the gas. This brings lower-metallicity gas from the outer parts of the galaxy to its centre, resulting in a lower metallicity in the central star-forming regions of the gas distribution. In principle, one could check the validity of this hypothesis by looking for statistical differences in the metallicity of BCGs with and without tidally induced star formation, or by detailed modelling of gas-rich mergers (e.g., Bekki 2008).

Regardless of how the SF is triggered, as far as the relationship between the gas distribution and regions of current SF is concerned, XMD BCGs do not appear to be qualita-

tively different from other late-type dwarf galaxies with low metallicities. For a sample of dwarf irregular galaxies (with metallicities mostly in XMD regime), Begum et al. (2006) find, much as we discuss above, that although SF generally occurs in regions of relatively high H I column density, there is no one-to-one relation between gas at high column density and H $\alpha$  emission. This lack of correspondence could be due to several effects, for example, ionization of the gas by UV radiation from H II regions could reduce H I column density in regions with strong H $\alpha$  flux. Further, since the massive star formation that the H $\alpha$  emission traces are short-lived, stochasticity in SF would also reduce the correlation between the instantaneous observed H $\alpha$  flux and the H I column density. It is also worth noting that, to the extent that one can determine a threshold density for SF, there does not seem to be any significant difference between XMD galaxies and the more metal-rich dwarfs in the Taylor et al. (1994) sample.

On the other hand, in the model of Schaye (2004) a lower limit to the threshold column density can be derived from the largest column densities outside the sites of current SF. In our galaxies this gas-density (corrected for inclination and with account of He) is  $\sim 2 \times 10^{21}$  atoms  $\text{cm}^{-2}$  for DDO 68 and UGC 772, and  $\sim 1.2\text{--}2.0 \times 10^{21}$  atoms  $\text{cm}^{-2}$  for J2104–0035 (as inclination of corresponding region is uncertain, gas-density may lie in the given range). For a proper comparison with more metal-rich galaxies, however, one would need to compare the column densities at a similar linear resolution.

Finally, we note that the baryonic masses of the XMD galaxies in our sample are all sufficiently large (greater than several  $10^8 M_\odot$ ), such that current star burst is not strong enough to cause a significant loss of metals through escape of metal-enriched gas (Fragile, Murray & Lin 2004). The low ISM metallicity of these galaxies could be due to a generally subdued star-formation rate in the past (in case of LSB galaxy progenitor). For those XMDs for which no tracers of old stellar population have so far been found in outer parts, the option of this interaction inducing the first SF episode remains a possibility.

## 7 SUMMARY

(i) All of the three XMD galaxies observed at the GMRT, viz., DDO 68, UGC 772 and SDSS J2104–0035 show disturbed morphology and velocity fields.

(ii) These distortions are suggestive of either an ongoing merging or tidal interaction with companions.

(iii) These results, taken together with existing H I data for I Zw 18 and SBS 0335–052 E and W, suggest that all six of the most metal-poor actively star-forming galaxies in the local universe are either merging or interacting objects.

(iv) Although SF generally occurs in regions of relatively high H I column density, there is no one-to-one relation between gas at high column density and H $\alpha$  emission. To the extent that one can determine a threshold density for SF, there does not seem to be any significant difference between these XMD galaxies and more metal-rich dwarf galaxies.

## ACKNOWLEDGMENTS

We thank the staff of the GMRT who have made these observations possible. The GMRT is run by the National Centre for Radio Astrophysics of the Tata Institute of Fundamental Research. Partial support for this work was provided by ILTP grant B-3.13, and through the Russian Foundation for Basic research grant 06-02-16617. Funding for the Sloan Digital Sky Survey (SDSS) and SDSS-II has been provided by the Alfred P. Sloan Foundation, the Participating Institutions, the National Science Foundation, the U.S. Department of Energy, the National Aeronautics and Space Administration, the Japanese Monbukagakusho, and the Max Planck Society, and the Higher Education Funding Council for England. The SDSS Web site is <http://www.sdss.org/>. The SDSS is managed by the Astrophysical Research Consortium (ARC) for the Participating Institutions. The Participating Institutions are the American Museum of Natural History, Astrophysical Institute Potsdam, University of Basel, University of Cambridge, Case Western Reserve University, The University of Chicago, Drexel University, Fermilab, the Institute for Advanced Study, the Japan Participation Group, The Johns Hopkins University, the Joint Institute for Nuclear Astrophysics, the Kavli Institute for Particle Astrophysics and Cosmology, the Korean Scientist Group, the Chinese Academy of Sciences (LAMOST), Los Alamos National Laboratory, the Max-Planck-Institute for Astronomy (MPIA), the Max-Planck-Institute for Astrophysics (MPA), New Mexico State University, Ohio State University, University of Pittsburgh, University of Portsmouth, Princeton University, the United States Naval Observatory, and the University of Washington.

## REFERENCES

- Aloisi A., Tosi M., Greggio L., 1999, *AJ*, 118, 302  
 Aloisi A., van der Marel R.P., Mack J., Leitherer C., Sirianni M., Tosi M., 2005, *ApJ*, 631, L45  
 Aloisi A. et al., 2007, *ApJ*, 667, L151  
 Begum A., Chengalur J.N., Karachentsev I.D., 2005, *A&A*, 433, L1  
 Begum A., Chengalur J.N., Karachentsev I.D., Kaisin S.S., Sharina M.E., 2006, *MNRAS*, 365, 1220  
 Bekki K., 2008, *MNRAS letters*, 388, 10  
 Carignan C., Purton C., 1998, *ApJ*, 506, 125  
 Chengalur J.N., Giovanelli R., Haynes M.P., 1995, *AJ*, 109, 2415  
 Chengalur J.N., Pustilnik S.A., Martin J.-M., Kniazev A.Y., 2006, *MNRAS*, 371, 1849  
 Elmegreen B.G., Kaufman M., Thomasson M., 1993, *ApJ*, 412, 90  
 Ekta, Chengalur J.N., Pustilnik S.A., 2006, *MNRAS*, 372, 853  
 Fragile P.C., Murray S.D., Lin D.N.C. 2004, *ApJ*, 617, 1077  
 Guseva N.G., Papaderos P., Izotov Y.I., Green R.F., Fricke K.J., Thuan T.X., Noeske K.G., 2003, *A&A*, 407, 105  
 Izotov Y.I., Thuan T.X., 2004, *ApJ*, 616, 768  
 Izotov Y.I., Thuan T.X., 2007, *ApJ*, 665, 1115  
 Izotov Y.I., Papaderos P., Guseva N.G., Fricke K.J., Thuan T.X., 2006, *A&A*, 454, 137  
 Kunth D., Östlin G., 2000, *A&ARv*, 10, 1  
 Momany Y., et al., 2005, *A&A*, 439, 111  
 Noeske K.G., Guseva N.G., Fricke K.J., Izotov Y.I., Papaderos P., Thuan T.X., 2000, *A&A*, 361, 33  
 Östlin G., 2000, *ApJ*, 535, L99  
 Östlin G., Kunth D., 2001, *A&A*, 371, 429  
 Östlin G., Amram P., Bergvall N., Masegosa J., Boulesteix J., Márquez I., 2001, *A&A*, 374, 800  
 Papaderos P., Izotov Y.I., Fricke K.J., Thuan T.X., Guseva N.G., 1998, *A&A*, 338, 43  
 Papaderos P., Fricke K.J., Thuan T.X., Izotov Y.I., Niklas H., 1999, *A&A*, 352, L57  
 Papaderos P., Izotov Y.I., Thuan T.X., Noeske K.G., Fricke K.J., Guseva N.G., Green R.F., 2002, *A&A*, 393, 461  
 Pustilnik S.A., Brinks E., Thuan T.X., Lipovetsky V.A., Izotov Y.I., 2001, *AJ*, 121, 1413  
 Pustilnik S.A., Kniazev A.Y., Lipovetsky V.A., Ugryumov A.V., 2001, *A&A*, 373, 24  
 Pustilnik S.A., Kniazev A.Y., Pramskij A.G., 2004, *A&A*, 425, 51  
 Pustilnik S.A., Kniazev A.Y., Pramskij A.G., 2005, *A&A*, 443, 91  
 Pustilnik S.A., Martin J.-M., 2007, *A&A*, 464, 859  
 Pustilnik S.A., Tepliakova A.L., Kniazev A.Y., 2008, *Astron. Lett.*, 31, 457  
 Sargent W.L.W., Searle L., 1970, *ApJ*, 162, L155  
 Schaye J., 2004, *ApJ*, 609, 667  
 Schaye J., 2007, preprint (astro-ph/0708.3366)  
 Schaye J., Dalla Vecchia C., 2008, *MNRAS*, 383, 1210  
 Schlegel D.J., Finkbeiner D.P., Davis M., 1998, *ApJ*, 500, 525  
 Skillman E.D., 1987, in *NASA Conf. Publ. Vol. 2466, Star Formation in Galaxies*, cWashington, p. 263  
 Smoker J.V., Davies R.D., Axon D.J., 1996, *MNRAS*, 281, 393  
 Smoker J.V., Davies R.D., Axon D.J., Hummel E., 2000, *A&A*, 361, 19  
 Springel V., Hernquist L., 2005, *ApJ*, 622, L9  
 Springel V., Di Matteo T., Hernquist L., 2005, *MNRAS*, 361, 776  
 Stil J.M., 1999, Ph.D. Thesis, Leiden University  
 Stil J.M., Israel F.P., 2002, *A&A*, 389, 29  
 Swarup G., Ananthakrishnan S., Kapahi V.K., Rao A.P., Subrahmanya C.R., Kulkarni V.K., 1991, *Current Science*, 60, 95  
 Taylor C.L., Brinks E., Pogge R.W., Skillman E.D., 1994, *AJ*, 107, 971  
 Thuan T.X., Izotov Y.I., Foltz C.B., 1999, *ApJ*, 525, 105  
 Tosi M., Aloisi A., Mack J., Maio M., 2006, eprint (astro-ph/0609659)  
 Tully R.B., Shaya E.J., Karachentsev I.D., Courtois H.M., Kocevski D.D., Rizzi L., Peel A., 2008, *ApJ*, 676, 184  
 van Zee L., Westpfahl D., Haynes M.P., Salzer J.J., 1998, *AJ*, 115, 1000  
 Zwicky F., 1965, *ApJ*, 142, 1293